

Measurements of Scatter Peaks in ^{137}Cs and ^{60}Co Sources

Leticia Pibida¹ and David West²

¹National Institute of Standards and Technology,
Gaithersburg, MD 20899, USA

²Oak Ridge National Laboratory,
Oak Ridge, TN 37830, USA

leticia.pibida@nist.gov
westdl@ornl.gov

Results from tests of radiation detection instruments with radionuclide identification capabilities will depend on the sources used for the tests. Radionuclide identification detectors are designed to measure photons and provide an identification of the source being measured. High-resolution spectra need to be acquired to determine all the observable peaks in the source spectra before testing these types of instruments. These peaks may be due to impurities and/or scatter peaks in the sources. This paper discusses the issues encountered with the response of a radioisotope identification device due to scatter peaks in one type of source used for testing. In addition, it provides spectra for different source types and source constructions to compare the differences in scatter, allowing for a better source type selection for instrument testing.

Key words: ANSI N42; radiation detection for homeland security; scatter peaks; source spectra; standards; testing of radiation detection equipment.

Accepted: May 18, 2018

Published: June 28, 2018

<https://doi.org/10.6028/jres.123.012>

1. Introduction

The Technical Test and Analysis Center (TTAC) at Oak Ridge National Laboratory (ORNL) conducts independent evaluations of radiation detection instrumentation. During one such test, the instrument under evaluation consistently generated an additional (erroneous) radionuclide identification. This became an area of concern for the following reasons:

- The raw data collected by the instrument contained an anomalous feature that could have contributed to the erroneous identification.
- The “complete and correct” data analysis guidelines in the American National Standards Institute (ANSI) N42.34 standard [1] consider the generation of additional erroneous radionuclides an incorrect identification, therefore determining that the instrument failed the radionuclide identification test.

The radioactive sources used for these measurements were originally designed to test radiation portal monitors against the requirements listed in the ANSI N42.35 standard [2]. Sources were designed to have a

thin stainless-steel encapsulation plate for its chemical resistance and mechanical strength, so that a source could tolerate the force of a vehicle driven over it without loss of radioactivity and have minimal gamma-ray attenuation. These sources were not designed for testing radioisotope identification devices (RIIDs).

2. Background Information from ORNL Measurements

The instrument under test at ORNL was a handheld RIID. The RIID tested was equipped with a $5.08 \text{ cm} \times 5.08 \text{ cm}$ NaI(Tl) detector. The specific test was a single radioisotope identification test, where the RIID identification capabilities are assessed using a set of gamma-ray emitting sources. Among these sources is ^{137}Cs , which emits a single gamma-ray energy of 662 keV. During testing with the ^{137}Cs source, the instrument occasionally identified ^{137}Cs together with ^{176}Lu , which, by complete and correct guidelines in the ANSI N42.34 standard [1], is considered an incorrect identification.

The raw gamma-ray spectrum collected by the instrument is shown in Fig. 1. The features in the spectrum are identified as follows:

- photopeak at 662 keV,
- Compton edge at approximately 480 keV, and
- edge of backscatter distribution at approximately 184 keV.

The center of the photon scattering region for the 662 keV gamma ray is expected at an energy of approximately 288 keV (labeled as “anomalous feature” in Fig. 1); see Sec. 3. The X-rays and gamma rays emitted by ^{176}Lu are listed in Table 1 [3], where uncertainties are combined standard uncertainties. Since ^{176}Lu emits gamma rays at energies close to 202 keV and 307 keV, it is possible that the backscatter peak combined with the edge of the backscatter distribution contributed to the erroneous identification of ^{176}Lu .

The source used during the single radionuclide identification testing was a stainless-steel disk source, examples of which are shown in Fig. 2. A detailed description of the stainless-steel disk source construction is given in Sec. 4.1. Figure 3 shows the source with the instruments under test.

Table 1. X-rays and gamma rays emitted by ^{176}Lu . Values were obtained from the Evaluated Nuclear Structure Data File (ENSDF) [3].

X-ray lines	Energy (keV)	Intensity
XR 1	7.9	0.231 ± 0.011
XR $k\alpha_2$	54.611	0.096 ± 0.003
XR $k\alpha_1$	55.79	0.166 ± 0.005
XR $k\beta_3$	62.985	0.0186 ± 0.0006
XR $k\beta_1$	63.243	0.0359 ± 0.0011
XR $k\beta_2$	64.942	0.0123 ± 0.0004
	88.34 ± 0.03	0.145 ± 0.006
	201.83 ± 0.03	0.780 ± 0.025
	306.78 ± 0.04	0.936
	400.99 ± 0.04	0.00037 ± 0.00004

A review of all the data collected during the testing revealed the following information about the peak at approximately 280 keV in the ^{137}Cs spectra:

- The peak was only evident in spectra from the stainless-steel disk source collected at exposure rates greater than or equal to $50 \mu\text{R/h}$ ($1.29 \times 10^{-8} \text{ C/kg/h}$).¹
- A ^{137}Cs button source (type D), in which the source is contained in a small plastic disk, did not display a peak at 280 keV.

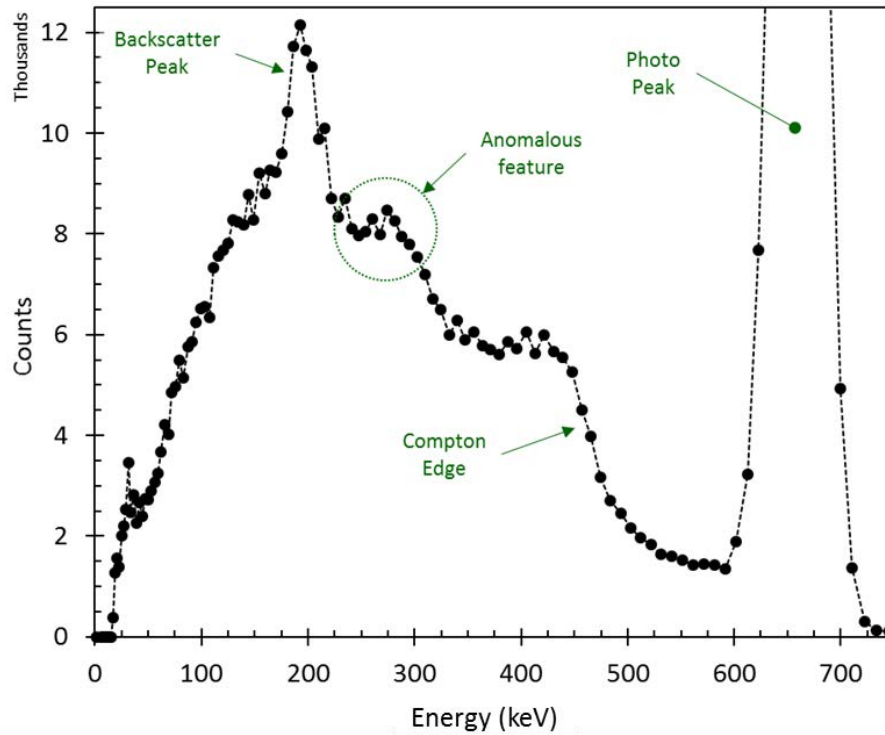


Fig.1. Gamma-ray spectrum collected by device under test.



Fig.2. Picture of stainless-steel plate sources.

¹ NIST does not endorse the use of non-SI units. This paper uses non-SI units because it addresses the requirements listed in the ANSI and Institute of Electrical and Electronics Engineers (IEEE) published standards.

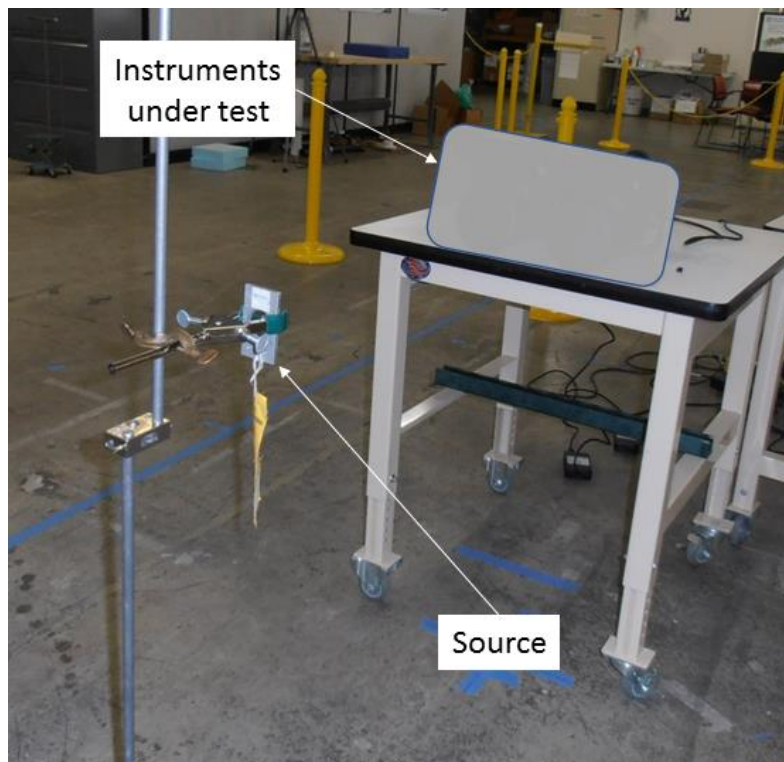


Fig. 3. Picture of test configuration at ORNL.

3. Motivation of NIST Measurements

Due to the results of the tests of the handheld RIID at ORNL using ^{137}Cs stainless-steel disk sources, NIST performed measurements using three different source construction types for ^{137}Cs and ^{60}Co sources to determine the differences in the spectral shapes.

For these measurements, both ^{137}Cs and ^{60}Co sources were used to determine and confirm the origin of the peak structure shown in Fig. 1. The energy of a scattered gamma ray can be calculated using the formula relating the photon deflection to the energy loss for Compton scattering [4, 5]:

$$E' = \frac{E}{1 + \left(\frac{E}{mc^2}\right)(1 - \cos \theta)} \quad (1)$$

where:

- E = photon energy before scatter;
- E' = photon energy after scatter;
- $mc^2 = 511$ keV, the electron rest energy; and
- θ = the photon deflection angle.

Scatter within the source can happen anywhere between the angles of $\theta = 0^\circ$ (forward emission) and $\theta = 180^\circ$ (backscatter). From Eq. 1, the 90° scatter peak ($\theta = 90^\circ$) for the 662 keV gamma ray of ^{137}Cs is expected to be observed at 288 keV. For the 1332 keV and 1173 keV gamma rays for ^{60}Co , the 90° scatter peaks ($\theta = 90^\circ$) are expected to be observed at 369 keV and 356 keV, respectively.

Several measurements were performed at NIST to determine the different source geometries and/or encapsulations that could potentially reduce the scatter peak observed in the ^{60}Co and ^{137}Cs stainless-steel disk sources, and the results are presented next.

4. Measurement Setup at NIST

Both NaI(Tl) and HPGe detectors were used to measure the spectrum from ^{60}Co and ^{137}Cs sources. The NaI(Tl) detector is 7.6 cm \times 7.6 cm (3 in. \times 3 in.), and the HPGe is a p-type coaxial detector 55.2 mm in diameter and 57.9 mm in length, with a 1.27 mm thick aluminum endcap.

Depending on the source activity, the center of the sources was placed at distances of 25 cm, 50 cm, and 100 cm from the front face of the detectors to be able to perform all measurements in a single day (to limit possible instrument and background fluctuations) and obtain a given number of counts in the main photopeak (counting times were kept between 10 min and 15 min). The sources used for the measurements are listed in Table 2, where uncertainties are combined standard uncertainties. Background spectra were acquired at the start and end of the measurements. The background spectrum was subtracted from the source spectra using the live-time to normalize the spectra.

Table 2. List of NIST-calibrated sources used for the measurements.

Radionuclide	Source type	Source number	Activity (MBq)	Reference time (EST)
^{137}Cs	Disk	NG 491	2.63 ± 0.13	30 September 2016, 12:00 h
	Cylindrical	P3-717	3.51 ± 0.11	1 April 2017, 15:00 h
	Point source	1545	0.01671 ± 0.00006	3 October 2002, 12:00 h
	Type D	11447-6	0.227 ± 0.007	16 September 2013, 12:00 h
^{60}Co	Disk	LL-17-60-1	1.66 ± 0.04	9 May 2017, 12:00 h
	Cylindrical	P3-715	3.37 ± 0.10	1 April 2017, 15:00 h
	Point source	07-0069-PS2	0.0951 ± 0.0003	5 August 2011, 12:00 h

Three different types of sources were used for these measurements, (1) stainless-steel disk sources, (2) stainless-steel cylindrical sources, and (3) point sources. For the ^{137}Cs , a type-D source was also used.

The ^{60}Co and ^{137}Cs stainless-steel disk sources were measured as a function of angle in 15° increments, with 0° being the flat face of stainless-steel disk facing the detector, and 90° being the aluminum frame facing the detector.

The cylindrical sources, point sources, and type-D source were measured at a single angle. The point sources and the type-D sources were measured with the flat face of the disk facing the detector. The cylindrical sources were mounted with the side wall facing the detector.

4.1 Stainless-Steel Disk Source Construction

These sources consist of filter paper loaded with radioactivity and sandwiched between two 316-type stainless-steel disks welded together at the edge (see Fig. 4; dimensions are given in Table 3). The stainless-steel disks are (0.254 ± 0.0127) mm thick [6]. The welded stainless-steel disks are placed inside an aluminum frame (see Fig. 5). This aluminum frame does not cover the active source area. The material of the source holder is 6061-T6 aluminum bar with dimensions of 3.175 mm \times 50.8 mm \times 88.9 mm and tolerance = ± 0.254 mm (unless otherwise indicated). Dimensional details for the disk and frame may be found in [6].

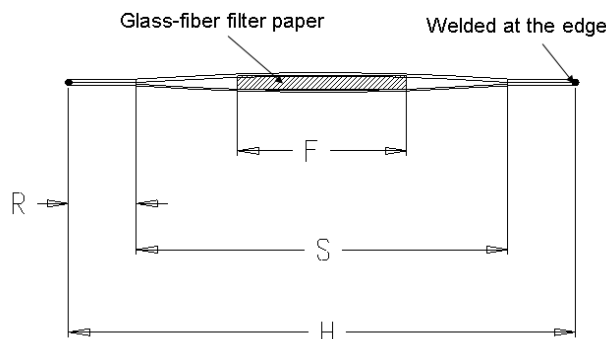


Fig. 4. Diagram of welded stainless-steel disk (see Table 3 for dimensions).

Table 3. Dimensions of stainless-steel disk source and aluminum frame.

Dimension	Values (mm)
F	12.70
H	38.10
R	5.08
S	27.94



Fig. 5. Picture of stainless-steel disk source placed inside the aluminum frame.

4.2 Stainless-Steel Cylindrical Source Construction

The cylindrical sources are double encapsulated in 304 stainless steel. The wall thickness is 1.295 mm. These sources were purchased from Eckert and Ziegler Isotope Products, and details about the source construction can be found in their catalog [7]. The source encapsulation type is A3011-4-1. A picture of this type of source is shown in Fig. 6. Viewed from the side, the radiation field emitted by the source has cylindrical symmetry.



Fig. 6. Picture of cylindrical source.

4.3 Point Source Construction

The point sources are small disks of filter paper (or a drop of solution) loaded with radioactivity and sandwiched between two pieces of plastic tape held by an aluminum ring. The filter paper (or solution drop) varies in diameter between 2 mm and 7 mm, depending on the source load. The aluminum ring has an inner diameter of 3.8 cm, an outer diameter of 5.4 cm, and a thickness of 0.64 mm (see Fig.7). The plastic tape is a 3M² #5 electrical tape that has a base layer that is 0.0254 mm thick polyester with an acrylic adhesive layer that is 0.0381 mm thick.

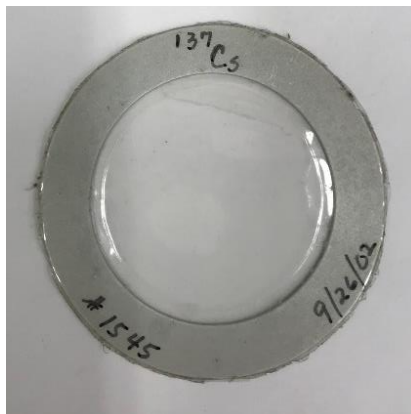


Fig. 7. Picture of point sources.

² Certain commercial equipment, instruments, or materials are identified in this paper to foster understanding. Such identification does not imply recommendation or endorsement by the National Institute of Standards and Technology, nor does it imply that the materials or equipment identified are necessarily the best available for the purpose.

4.4 Type-D Source Construction

The type-D disk source is a 25.4 mm diameter by 6.35 mm thick disk constructed of high-strength plastic; see Fig.8. The active diameter is 5 mm. This source is asymmetric and is designed to be used from the smooth plastic side (opposite to the source label side) that is 2.77 mm thick. Information about the source encapsulation can be found in the Eckert and Ziegler Isotope Products catalog [7].



Fig. 8. Picture of type-D source.

5. Measurement Results

5.1 ^{60}Co Measurements

The results of the ^{60}Co stainless-steel disk source measurements using an HPGe detector for different source angles are shown in Fig. 9 and Fig.10. The Compton edge and the end of the backscatter distribution are marked in Fig. 9. Figure 10 is a close-up view of Fig. 9 for the energy region between 200 keV and 1350 keV. In Fig. 10, a broad peak around 352 keV with a full width half maximum (FWHM) of 33.2 keV at a 0° angle and a smaller and broader peak for the 15° angle are observed. At the gamma-ray energy of 352 keV, a photopeak will have a FWHM of approximately 1 keV. Additional measurements using the ^{60}Co cylindrical and point sources were acquired with the same detector. Results are shown in Fig. 11, together with the stainless-steel disk source measurement at the 0° angle. In Fig. 11, single and double escape peaks are observed in the cylindrical source spectrum. The scatter peak is not observed in the point source, as expected due to the low-scatter type of material used in the construction of this kind of source. The scatter peak is not observed in the cylindrical source either because of the source construction or because of the orientation of the source with respect to the detector.

For stainless-steel disk source, the observed source intensity varies sharply for the 90° angle, so testing of radiation detection instruments such as RIIDs should not be performed with the source in this orientation, because a small deviation from the 90° angle would produce a different radiation field at the detector. This could lead to test results that would be inaccurate because the actual radiation field might be different from the expected value in an uncontrolled way.

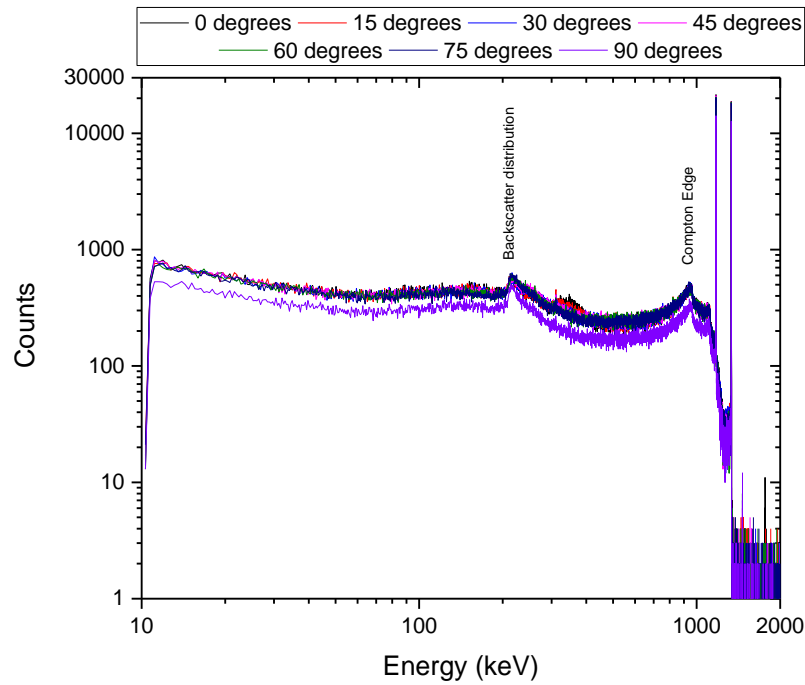


Fig. 9. ^{60}Co stainless-steel disk source measurements using an HPGe detector for different source angles.

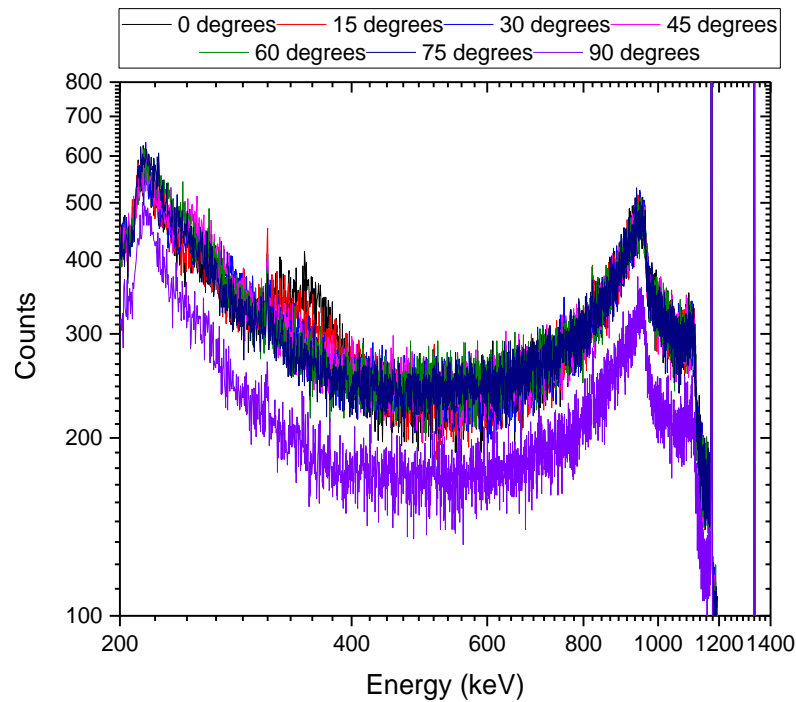


Fig. 10. Close-up view of the 200 keV to 1350 keV energy region of Fig.9.

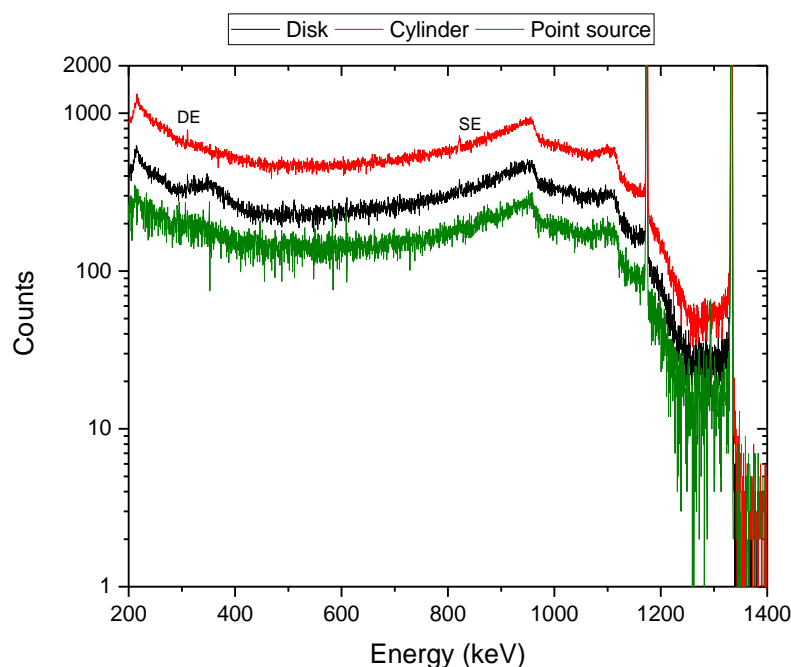


Fig. 11. HPGe measurements using the ^{60}Co cylindrical and point sources together with the stainless-steel disk source measurement at the 0° angle.

In addition to the HPGe measurements, measurements were made using a NaI(Tl) detector for the stainless-steel disk source at 0° and 90° angles, and for the cylindrical and point sources at a 0° angle. NaI(Tl) spectra are shown in Fig. 12 and Fig. 13. From Fig. 12, a reduction in the $\sim 90^\circ$ angle scatter peak can be observed when the source aluminum frame is facing the detector. When the flat surface of the disk source is facing the detector (0° angle), the attenuation of the scatter peak through the disk is small, as the wall thickness is only 0.254 mm. In addition, there is more material from which photons can scatter at a 90° angle due to the presence of the source frame. When the aluminum frame is facing the detector, the scatter photons need to pass through the encapsulation and frame material and cover a longer path compared to the 0° angle. Additionally, there is less material at a 90° angle (due to the presence of the thin stainless-steel disk) from which the photons can scatter. Consequently, the scatter photon intensity is reduced. As the scatter source intensity is reduced at the 90° angle, the intensity of the main gamma ray is also reduced, due the material surrounding the radioactive material. The FWHM of the scatter peak is approximately 62 keV. From Fig. 13, it can be observed that the scatter radiation produced in the point source is the smallest of all sources. For the cylindrical source, even if the broad scatter peak is not observed, the scatter radiation contribution is larger than that observed in the point source spectrum.

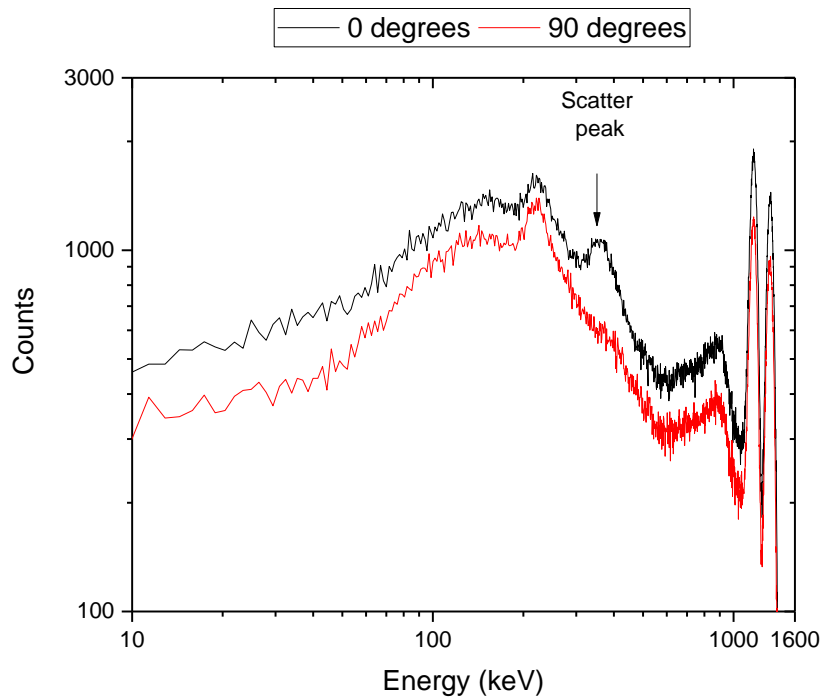


Fig. 12. ^{60}Co stainless-steel disk source measurements using an NaI(Tl) detector for 0° and 90° angles.

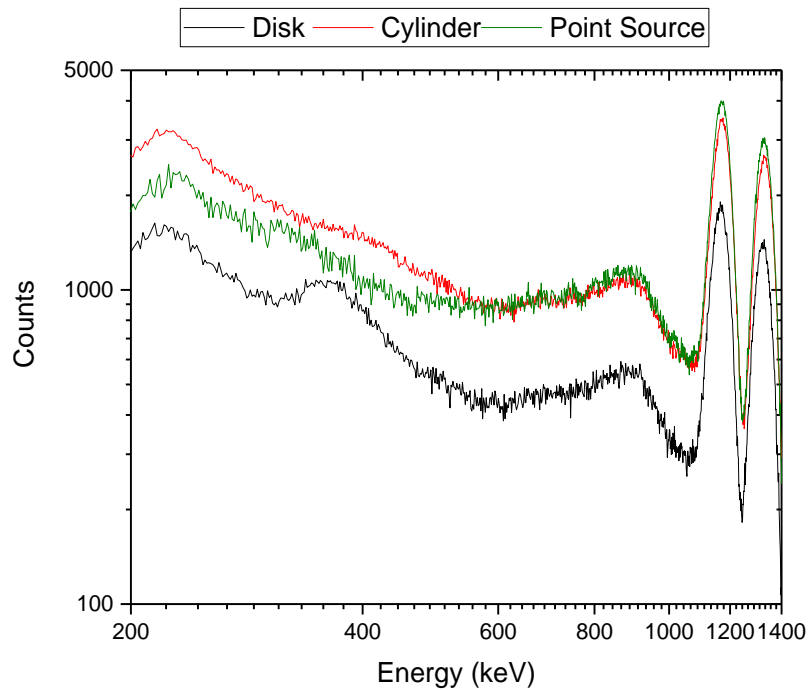


Fig. 13. NaI(Tl) measurements using the ^{60}Co cylindrical and point sources together with the stainless-steel disk source measurement at a 0° angle.

5.2 ^{137}Cs Measurements

The results of the ^{137}Cs stainless-steel disk source measurements using an HPGe detector for different source angles are shown in Fig. 14 and Fig. 15. The Compton edge and the end of the backscatter distribution are marked in Fig. 14. Figure 15 is a close-up view of Fig. 14 for the energy region between 150 keV and 700 keV. From these measurements, the scatter peak can be observed at an energy of approximately 280 keV, but only for the 0° angle measurement with a FWHM of approximately 35 keV. Figure 16 shows the spectra for the disk, cylindrical, type-D, and point sources at a 0° angle. The scatter peaks are not observed in the cylindrical and point sources. Scatter peaks at slightly different energies can be observed for the disk and type-D sources (as marked by the arrows in Fig. 16).

For stainless-steel disk source, the observed source intensity varies sharply for the 90° angle, so testing of radiation detection instruments such as RIIDs should not be performed with the source in this orientation, because a small deviation from the 90° angle would produce a different radiation field at the detector. This could lead to inaccurate test results because the actual radiation field might be different from the expected value in an uncontrolled way.

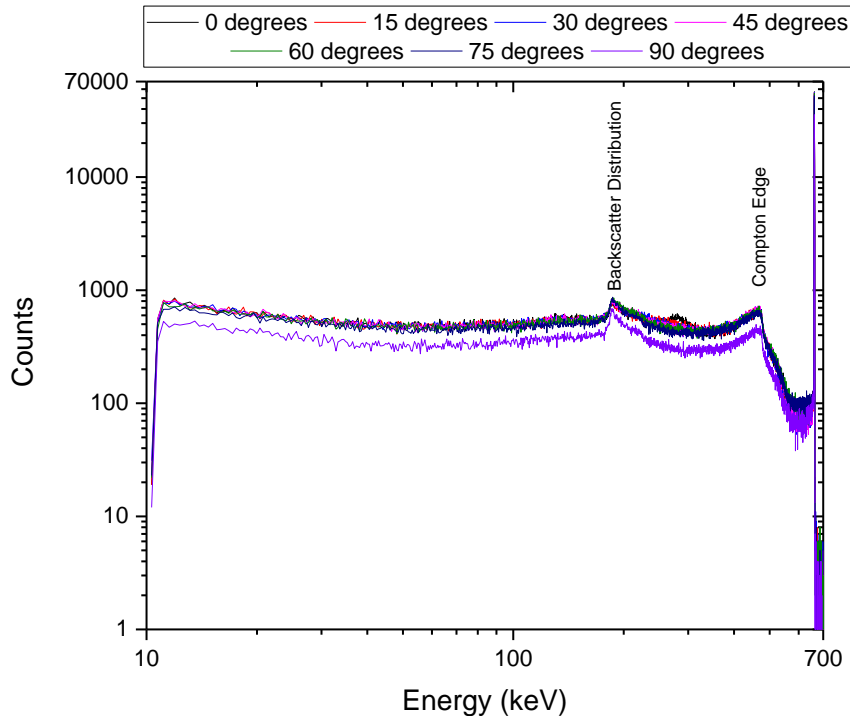


Fig. 14. ^{137}Cs stainless-steel disk source measurements using an HPGe detector for different source angles.

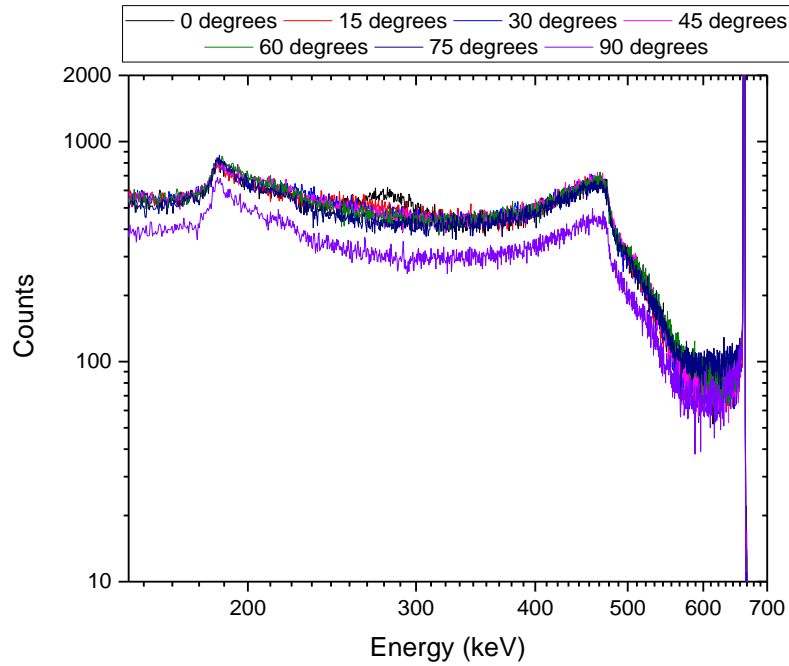


Fig. 15. Close-up view of the 150 keV to 700 keV energy region of **Error! Reference source not found.**

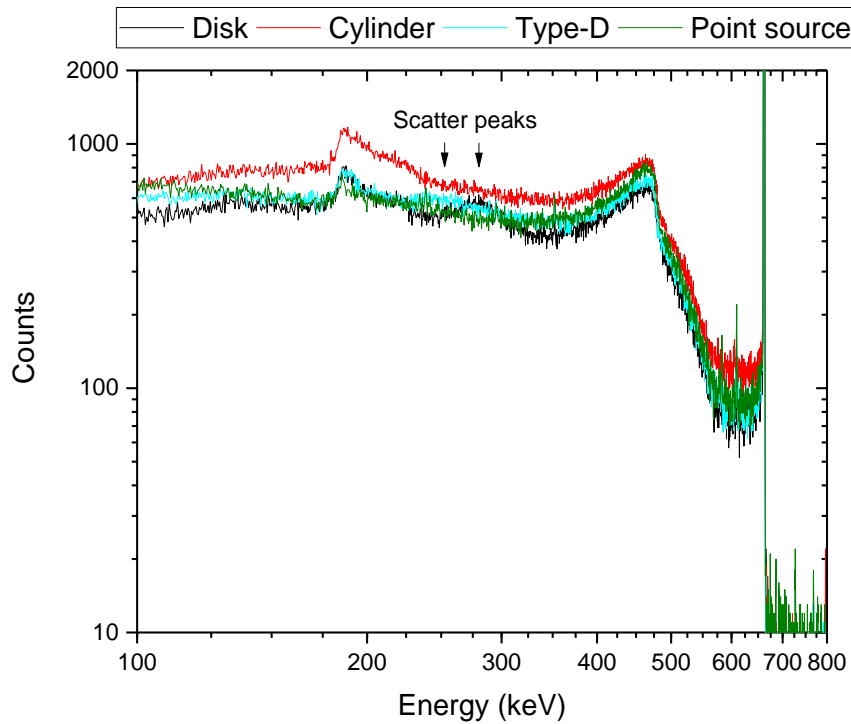


Fig. 16. HPGe measurements using the ^{137}Cs cylindrical, point source, type-D, and stainless-steel disk sources at a 0° angle.

Measurements using the NaI(Tl) detector were also made using the stainless-steel disk source at 0° and 90° angles, and the cylindrical source at a 0° angle. The NaI(Tl) spectra are shown in Fig. 17 and Fig. 18. For the cylindrical source, a broader and weaker scatter peak was observed in the spectrum. As the thickness of the stainless-steel disk is very thin, the X-ray emission between 31 keV and 37 keV was measured at the 0° angle. The FWHM of the 90° scatter peak is approximately 44 keV.

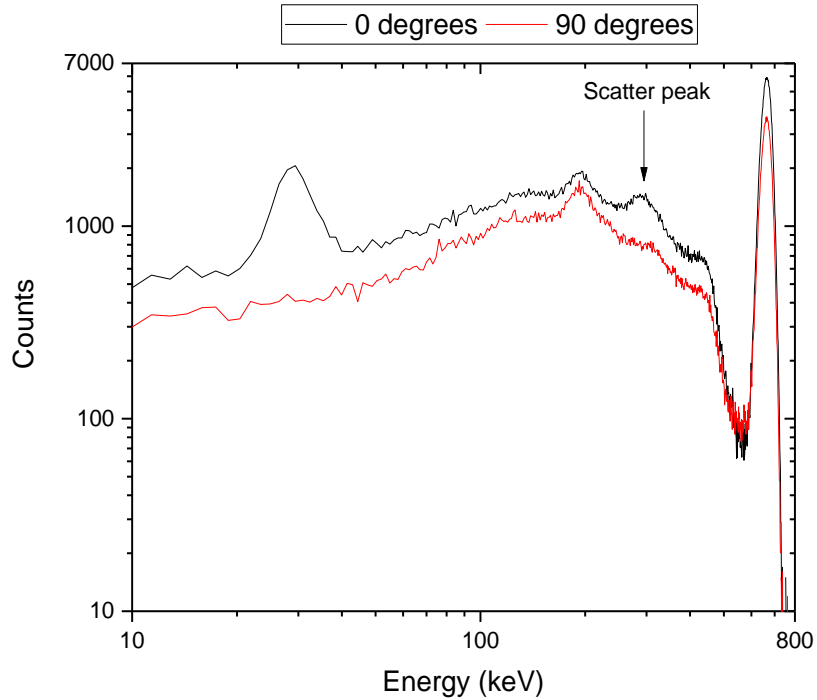


Fig. 17. ¹³⁷Cs stainless-steel disk source measurements using an NaI(Tl) detector for 0° and 90° angles.

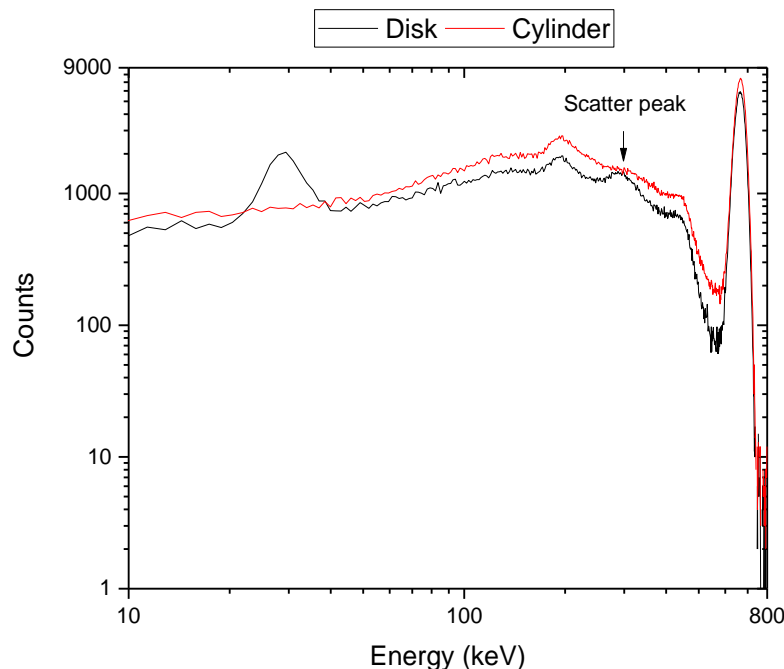


Fig. 18. NaI(Tl) measurements using the ^{137}Cs cylindrical and stainless-steel disk source at a 0° angle.

6. Conclusions

For the HPGe measurements, a scatter peak was observed for the ^{60}Co stainless-steel disk at 0° and 15° angles. The disk source has additional attenuating material at a 90° angle due to the presence of the frame, away from which the photons can scatter. This is not observed for the cylindrical source and the point source. For the point source, it is not observed because the source is very thin, and there is no material from which the photons to scatter. The source construction of the cylindrical source reduces the scatter peak. In addition, the wall thickness of the cylindrical source is larger than that of the disk source, so scatter photons could be attenuated as they travel through the source volume and encapsulation walls. When measuring the same sources with the NaI(Tl) detector, a scatter peak was observed for the disk source, and additional scatter was observed for the cylindrical source compared to the point source.

For the ^{137}Cs stainless-steel disk, the scatter peak was observed at a 0° angle and at a lower energy, as expected. Similar behavior was observed for the different types of sources as for the ^{60}Co sources. Both the type-D and disk sources displayed scatter peaks at slightly different energies. For the HPGe measurements, the scatter peaks were approximately 30 times wider than a photopeak at the same gamma-ray energy.

The observed source intensity varied sharply for the 90° angle, so testing of radiation detection instruments such as RIIDs should not be performed with the source in this orientation, because a small deviation from the 90° angle may produce a different radiation field at the detector, and this could lead to inaccurate test results, as the actual radiation field might be different from the expected value.

Before testing instruments with radionuclide identification capabilities, such as RIIDs, it is recommended that high-resolution spectra be acquired for all sources used in the tests. All peaks in the spectra should be identified and associated with radionuclides that are present in the instrument library in order to determine the acceptable instrument response. Based on the data obtained for this work, without an awareness of and consideration of scatter peaks or peaks due to impurities, instrument testing results may display apparently unacceptable results that could be expected based on the instrument's library.

7. References

- [1] ANSI (2015) *ANSI N42.34-2015—American National Standard Performance Criteria for Handheld Instruments for the Detection and Identification of Radionuclides* (American National Standards Institute, Washington, D.C.). <https://doi.org/10.1109/IEEESTD.2016.7551091>
- [2] ANSI (2016) *ANSI N42.35—American National Standard for Evaluation and Performance of Radiation Detection Portal Monitors for Use in Homeland Security* (American National Standards Institute, Washington, D.C.). <https://doi.org/10.1109/IEEESTD.2016.7551097>
- [3] Basunia MS (2006) Nuclear Data Sheets 107, 791. Evaluated Nuclear Structure Data File (ENSDF). National Nuclear Data Center (NNDC), Brookhaven National Laboratory, Upton, New York. Available at <http://www.nndc.bnl.gov/>
- [4] Hubble JH (August 1969) Photon Cross Sections, Attenuation Coefficients and Energy Absorption Coefficients from 10 keV to 100 GeV. National Bureau of Standards, Washington, D.C., National Standard Reference Data System NSRDS-NSB 29. <http://dx.doi.org/10.6028/nbs.nsrds.29>
- [5] Nelson G, Reilly D (1991) Gamma-ray interactions with matter. *Passive Nondestructive Assay of Nuclear Materials*, eds Reilly D, Ensslin N, Smith H Jr (U.S. Nuclear Regulatory Commission, Washington, D.C.).
- [6] Lucas L, Pibida L, Unterweger M, Karam L (2005) Gamma-ray emitting test sources for Portal Monitors used for homeland security. *Radiation Protection Dosimetry* 113(1):108–111. <https://doi.org/10.1093/rpd/nch422>
- [7] On-line Eckert and Ziegler Isotope Products. Available at https://www.ezag.com/fileadmin/user_upload/isotopes/isotopes/Isotrak/isotrak-pdf/Product_literature/EZIPL/EZIP_catalogue_reference_and_calibration_sources.pdf

About the authors: *Leticia Pibida is a physicist in the Radiation Physics Division at NIST. David West is an R & D staff researcher in the Electrical and Electronic Systems Research Division at ORNL. The National Institute of Standards and Technology is an agency of the U.S. Department of Commerce.*